Physics and Imaging in Radiation Oncology 11 (2019) 21–26

Contents lists available at ScienceDirect

Physics and Imaging in Radiation Oncology

journal homepage: www.elsevier.com/locate/phro

Original Research Article

Development and accuracy evaluation of a single-camera intra-bore surface scanning system for radiotherapy in an O-ring linac

Laurence Delombaerde[a,b], Saskia Petillion[a], Steven Michiels[a,b], Caroline Weltens[a,b], Tom Depuydt[a,b,*]

[a] Department of Radiation Oncology, University Hospitals Leuven, Herestraat 49, Leuven 3000, Belgium
[b] Department of Oncology, KU Leuven, Herestraat 49, Leuven 3000, Belgium

ARTICLE INFO

Keywords:
Surface scanning
SGRT
Closed-bore linac
Motion monitoring

ABSTRACT

Background and purpose: Current commercial surface scanning systems are not able to monitor patients during radiotherapy fractions in closed-bore linacs during adaptive workflows. In this work a surface scanning system for monitoring in an O-ring linac is proposed.

Methods and materials: A depth camera was mounted at the backend of the bore. The acquired surface point cloud was transformed to the linac coordinate system after a cube detection calibration step. The real-time surface was registered using an Iterative Closest Point algorithm to a reference region-of-interest of the body contour from the planning CT and of a depth camera surface acquisition from the first fraction. The positioning accuracy was investigated using anthropomorphic 3D-printed phantoms with embedded markers: a head, hand and breast. To simulate clinically observed positioning errors, each phantom was placed 24 times with 0–10 mm and 0–8° offsets from the planned position. At every position a cone-beam CT (CBCT) was acquired and a surface registration performed. The surface registration error was determined as the difference between the surface registration and the CBCT-to-CT fiducial marker registration.

Results: The registration errors were (mean ± SD): lat: 0.4 ± 0.8 mm, vert: −0.2 ± 0.2 mm, long: 0.3 ± 0.5 mm and Yaw: −0.2 ± 0.6°, Pitch: 0.4 ± 0.2°, Roll: 0.5 ± 0.8° for the body contour reference, and lat: −0.7 ± 0.7 mm, vert: 0.3 ± 0.2 mm, long: 0.2 ± 0.5 mm and Yaw: −0.5 ± 0.5°, Pitch: 0.1 ± 0.3°, Roll: −0.7 ± 0.7° for the captured surface reference.

Conclusion: The proposed single camera intra-bore surface system was capable of accurately detecting phantom displacements and allows intrafraction motion monitoring for surface guided radiotherapy inside the bore of O-ring gantries.

1. Introduction

Accurate and reproducible patient positioning is of major importance in current highly conformal radiotherapy. The use of narrow margins around the clinical target volume and the introduction of high dose gradient intensity-modulated radiotherapy (IMRT) treatments require exact knowledge of tumor and organs-at-risk positions [1]. Image guided radiotherapy (IGRT) has become the standard to verify and adapt patient position. Planar X-ray imaging or cone-beam CT (CBCT) are frequently employed for setup verification and/or intrafraction monitoring resulting in an additional radiation dose to the patient [2]. In the last 10 years there has been increasing interest in supplementing IGRT with optical surface scanning technology for patient positioning and monitoring during treatment. Surface scanning technology is based on laser interferometry or structured light stereovision. It acquires the 3D skin surface of the patient, which is registered to a reference, usually the body contour from the planning CT, to aid in accurate positioning and monitoring stability during treatment delivery. An improved setup accuracy compared to skin tattoos has been shown for a range of indications, from breast, intracranial stereotactic radiosurgery to extremities [3–6]. Furthermore, surface guidance for breast breath-hold treatments has been shown to have a good correlation to CBCT [7,8] or portal images [9].

Commercially available systems use 3 ceiling mounted pods to reconstruct the patients topography. On conventional C-arm linear accelerators these systems are focused on the isocenter. The pods are mounted to the treatment room ceiling in an optimal configuration to have a lateral view of the patient and offer some redundancy toward

* Corresponding author at: Department of Radiation Oncology, University Hospitals Leuven, Herestraat 49, Leuven 3000, Belgium.
E-mail address: tom.depuydt@kuleuven.be (T. Depuydt).

https://doi.org/10.1016/j.phro.2019.07.003
Received 15 April 2019; Received in revised form 28 June 2019; Accepted 3 July 2019

blocking of the camera view by the gantry arm or gantry-mounted imaging source and detector for certain gantry angles. On C-arm gantries the patients are set up at the isocenter. For O-ring gantry systems, setup of the patient is performed in front of the bore at a setup isocenter, as access to the patient inside the bore at the treatment isocenter is limited. Surface scanning systems can be used to guide patient setup at this setup isocenter, however after translation to the treatment isocenter in the gantry bore, the patient can no longer be monitored with the ceiling mounted system. As a consequence, detecting intrafraction movement during stereotactic body radiation therapies (SBRT) with long beam-on times and surface-guided deep-inspiration breath-hold (DIBH) treatments are severely restricted on O-ring gantries. Furthermore, with the advent of online adaptive workflows, monitoring the patient during the additional time required for – online contouring, replanning and decision making – is essential to ensure the validity of the adaptation. Typically this procedure can take from 15 up to 45 min.

Multiple researchers have developed in-house surface scanning solutions on C-arm linacs. Gaisberger et al. [10] used 2 ceiling mounted pods for setup of breast cancer patients. Gilles et al. [11] developed a surface scanning system with 2 ceiling mounted pods as well, to detect patient displacements for lung, pelvic and head & neck cancer patients. These solutions are mounted to the ceiling and possibly face the same limitations as the commercial systems, a view of the patient would be lost while at the treatment isocenter for O-ring systems.

Given these current limitations of both commercial and in-house systems we have developed a compact single-camera system for motion monitoring at the treatment isocenter in enclosed bore gantries. A gaming industry electronics device, which has been implemented in the medical field from respiratory tracking and motion detection in positron emission tomography (PET) [12,13] and radiotherapy [14,15] to patient-gantry collision detection [16], was selected for this purpose. In this work a surface scanning system was developed and the accuracy validated using a set of 3 anthropomorphic 3D-printed phantoms.

2. Methods

2.1. In-room camera setup and camera calibration

A Kinect for Windows v1 (Microsoft) was selected as the depth camera sensor due to its accessible open developer toolkit. The sensor uses structured light technology to retrieve depth information working distance of 0.5–4 m, compatible with the intra-bore geometry. The Kinect was connected to a computer (2.00 GHz Intel i5 CPU, 8 GB RAM), and analysis was performed in MATLAB 2017b (The MathWorks, US). To determine the optimal camera position relative to the linacs isocenter, the Kinect's depth sensitivity was determined.

The camera was placed on the treatment couch perpendicular to a flat board at distances 70, 80, 90 and 100 cm and the couch was shifted with 1 mm increments from 0 to 5 mm with a displacement accuracy of < 0.5 mm. For every step 100 depth frames were collected. A central region of 150×150 pixels was averaged over all frames and the expected depth signal was compared to the measured one.

The sensor was positioned centrally at the back-end of the bore of a Halcyon linac (Varian Medical Systems, US) at a distance of 85 cm from the radiation isocenter at a 45° angle to the treatment couch, as illustrated in Fig. 1, following the depth sensitivity tests. Transforming the acquired 3D point cloud to the linac coordinate system was performed via a method similar to Gilles et al. [11]. A polystyrene cube ($15 \times 15 \times 15\,cm^3$) (QA phantom, VisionRT) was positioned diagonally on the treatment couch with the center of the cube at isocenter. The position was verified with MV-CBCT by detecting 5 ceramic spheres embedded in the phantom. The 3D scene was reconstructed by averaging 5 subsequently acquired point clouds for noise suppression. The 3 visible cube edges in the reconstructed point cloud were retrieved by an automated registration procedure, giving the transformation of the depth camera coordinate system to the linac coordinate system. Due to the dependence of positioning accuracy on the geometric calibration of the camera system, the calibration procedure was tested for stability. After correct positioning of the cube, 100 consecutive calibrations were performed, while leaving the cube unaltered to determine the stability of the cube detection method. The 3D standard deviation and the maximal deviation for all 100 isocenter positions from the average position, as retrieved by the depth sensor, were reported. This procedure was repeated on 5 different days to detect any sensitivity to the specific setup of the day as the Kinect was mounted on a mobile setup. All measurements were performed after the necessary warm-up time of the sensor to reach a stable depth signal.

2.2. Development of surface scanning system

After sensitivity characterization and geometric calibration of the depth sensor, a surface scanning system was developed in MATLAB combining the depth camera system with surface acquisition and registration software, called the Compact Intra-bore Surface Scanner (CISS) hereafter. Following pre-processing, the real-time generated surface was stored to the hard drive and registered to the body contour from the planning CT using a point-based registration. Offline, the real-time surface was registered to a surface scanning capture reference taken while at the treatment position. The workflow of the system is shown in Supplementary Fig. 1.

The reference surface was either (a) the body contour for the planning CT of the 3D-printed anthropomorphic phantom (as further described in Section 3.1) or (b) a captured surface reference taken by the CISS at the first fraction.

The anthropomorphic phantoms were scanned on a Siemens Sensation Open at 120 kVp with slice thickness 1.5 mm. The body contour was segmented by thresholding (lower limit: −800 HU), with manual corrections. A dummy plan was added in the Treatment Planning System (TPS) (Eclipse, Varian Medical Systems) to fix an isocenter in the phantom. The structure set containing the body contour was then imported into the MATLAB software. A region of interest (ROI) was selected by the user during the first fraction. A 3D point cloud was created from the surface mesh by using the vertices only. This point cloud was downsampled to 8 points per cm^3 by discretization of the point cloud using a box grid, and averaging all points lying in a box to the centroid position, to improve computational efficiency.

For every phantom, a capture reference surface was created by the CISS when at the treatment position during the first fraction. Two depth frames were acquired and a merged point cloud created. A ROI was selected excluding elements not part of the phantom, e.g. the couch.

The real-time data was generated by acquiring 2 consecutive depth frames from the sensor and creating a merged 3D point cloud. The field of view was limited to a volume of $70 \times 100 \times 120\,cm^3$ (lateral × vertical × longitudinal) around the isocenter. The treatment couch was removed by a MATLAB native RANSAC plane fitting method [17]. The remaining point cloud was transformed to the linac coordinate system by multiplying with the transformation matrix retrieved from the calibration, as discussed Section 2.1. Finally the point cloud was downsampled using a box grid approach to decrease noise and achieve a uniform spatial sampling comparable to the reference (8 points per cm^3). The real-time data was then stored and registered to the body contour reference with an Iterative Closest Point algorithm to determine the offset from the planned position.

A modified form of the Iterative Closest Point (ICP) algorithm by Besl and McKay [18] was used to rigidly align the live surface to the reference. The objective was to minimize mean squared error E between a transformed point cloud and the reference by iteratively updating the 6 degrees-of-freedom (DOF) rigid transformation (R, T):

$$E(R, T) = \frac{1}{N} \sum_{i=1}^{N} \|a_i - R \cdot b_i - T\|^2$$

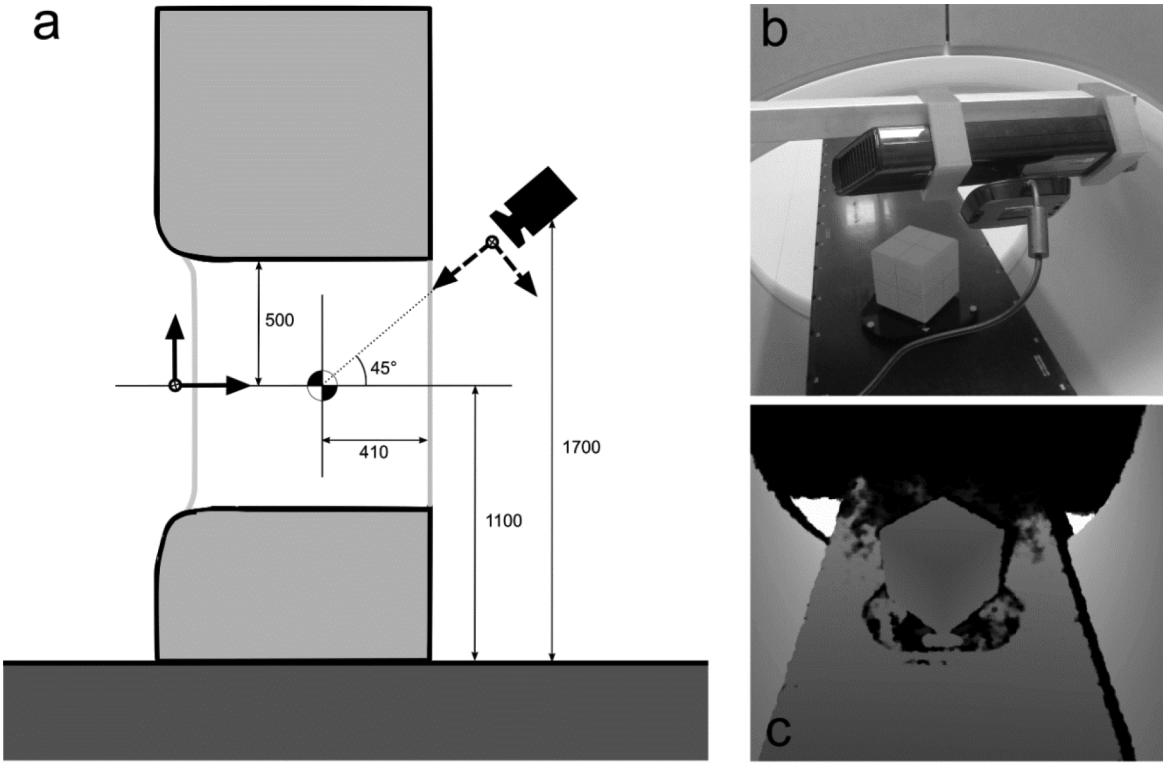

Fig. 1. (a) Illustration of the depth camera's position relative to linac isocenter. Distances (in mm) indicated as a reference. Sensor's dimensions not to scale. The camera's coordinate system is indicated with dashed arrows, the couch axes with solid arrows. (b) Photograph of the Kinect mounted on the movable rack. (c) Depth view of the calibration cube from the sensor's position.

where a_i and b_i are corresponding points in the real-time and reference point cloud resp. An implementation by Birdal [19] of the Picky ICP [20] which selects corresponding points in a multi-hierarchical strategy to increase robustness to outliers and improve computation times, was used.

2.3. Accuracy evaluation with 3D-printed anthropomorphic phantoms

To evaluate the registration accuracy of the surface scanning system, a set of rigid anthropomorphic phantoms were generated covering a range of relevant surface complexity (Fig. 2). A hand, head and breast were printed in polylactic acid (ICE Filaments, Belgium) on a Raise3D N2 Plus 3D-printer (Raise3D, The Netherlands). The breast phantom was constructed from the contoured breast volume in a patient's CT scan. The head and hand phantom were freely available models, retrieved from [21,22] respectively. In every model 10 strategically distributed cavities were added during the 3D-printing process in which 2.5 mm diameter lead markers (Suremark, US) were inserted. The breast phantom was attached to the E2E SBRT Thorax phantom (CIRS, US) to recreate realistic circumstances for the breast's position.

The accuracy of the surface scanning system was tested by simulating clinically observed positioning errors. Each phantom was positioned 24 times randomly to within approximately 10 mm from the isocenter and allowing some level of rotation. An MV-CBCT ($1.08 \times 1.08 \times 1.99\,mm^3$ voxel size) was acquired and registered offline to the planning CT using a fiducial marker matching. An automated registration was performed by extracting the centers of the spherical lead markers in both CT and CBCT images with a 3D Hough transform [23,24] and calculating the transformation between both sets of centers with Horn's quaternion method [25], using 3DSlicer [26]. The accuracy of this procedure was tested by comparing the automated registration result to a known applied transformation to preregistered CBCTs. The error was found to be < 0.01 mm and $< 0.01°$.

At every phantom position the prototype surface scanning system performed an ICP registration to the body contour reference ROI. The surface scanning registration error (RE) was determined by calculating the difference between this ICP transformation and the transformation from the fiducial marker registration:

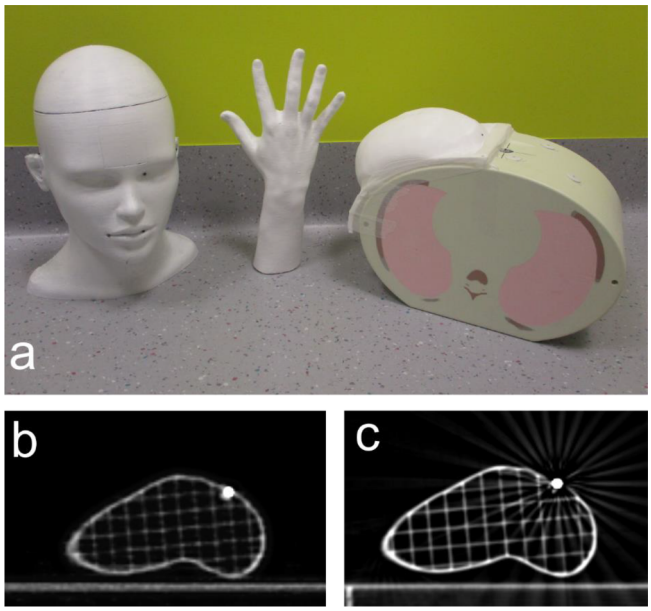

Fig. 2. (a) Photograph of the 3 anthropomorphic phantoms used in the accuracy evaluation of the surface scanning prototype. Head, hand and breast phantom were painted white and 10 lead markers inserted in evenly distributed cavities. The breast phantom is taped to the CIRS Thorax SBRT E2E phantom. (b) An axial slice of the hand phantom MV-CBCT at a lead marker position. (c) Planning CT slice at the same marker position.

$$RE_{translation} = \boldsymbol{t}_{surface\ scanning} - \boldsymbol{t}_{CBCT-CT}$$

$$RE_{rotation} = r_{surface\ scanning} - r_{CBCT-CT}$$

Offline, the surface registration was repeated by registering the real-time surface to the captured reference surface. The RE was calculated for this capture reference as described above.

3. Results

3.1. Depth sensitivity

Depth increments of 1 mm were accurately detected for distances larger than 70 cm. The largest error was detected as 1.1 mm for a 1 mm shift at 70.4 cm as shown in Supplementary Fig. 2. For camera distances of 80, 90 and 100 cm the errors were reduced to below 0.4 mm. Following these results the depth camera was placed at a distance of 85 cm from the isocenter at the back-end of the bore.

3.2. Geometric calibration stability

For the 100 calibrations, repeated 5 times on different days where the surface scanning system was repositioned to check for sensitivity to the camera position, the standard deviation (vector norm) from the mean position of the retrieved isocenter position is shown in Table 1. The maximum 3D distance between 2 retrieved isocenters is also given.

3.3. Accuracy evaluation using anthropomorphic phantoms

The mean and standard deviation of the RE of the surface scanning prototype compared to CBCT using both the body contour reference and the captured reference are given in Table 2.

The combined registration errors of the 3 phantoms to the CBCT reference were (mean ± SD): lat: 0.4 ± 0.8 mm, vert: −0.2 ± 0.2 mm, long: 0.3 ± 0.5 mm and Yaw: −0.2 ± 0.6°, Pitch: 0.4 ± 0.2°, Roll: 0.5 ± 0.8° for the body contour reference, and lat: −0.7 ± 0.7 mm, vert: 0.3 ± 0.2 mm, long: 0.2 ± 0.5 mm and Yaw: −0.5 ± 0.5°, Pitch: 0.1 ± 0.3°, Roll: −0.7 ± 0.7° for the surface capture reference. The maximum RE found was 2.4 mm in the longitudinal direction for the head phantom and 2.5° for the pitch rotation for the breast phantom for the body contour reference. Using the capture reference surface, the largest errors were found for the breast phantom where the lateral component deviated 3.6 mm and for another fraction the roll component 3.0°.

The detected displacement versus the CBCT reported displacement is shown in Fig. 3 for the translations of the body contour reference. No correlation was found between the registration error and the displacement magnitude, both for translations and rotations, all p values > 0.01 (*t*-test).

4. Discussion

The emergence of closed-bore gantry linacs has a major impact on the applicability of ceiling mounted surface scanners. The current configuration of multiple vendors limits their use in closed-bore gantries. Implementing motion management strategies for breath-hold treatments or online adaptive workflows are therefore severely restricted. This work proves that by developing a compact surface scanning solution, monitoring inside an O-ring closed bore gantry is feasible. Our surface scanning prototype uses a similar workflow as the commercial systems – scan the patient, create a body contour, register the real-time surface to reference – but is kept as compact as possible to be able to be used in the confined space of the O-ring bore.

Table 1
The standard deviation (and maximal deviation) of the retrieved isocenters from the mean position for 100 consecutive calibrations, repeated on 5 days where the surface scanning system was repositioned.

	Day 1	Day 2	Day 3	Day 4	Day 5
Standard Deviation (mm)	0.0	0.1	0.1	0.0	0.1
Maximum (mm)	0.5	0.7	0.6	0.3	0.5

The system achieved an accuracy below the recommended accuracy of Task Group Report 147, namely < 2 mm for surface guided technology (no rotational error is given in the report) for standard dose fractionation regimens [27]. A direct comparison of the accuracy to previous studies on non-commercial surface scanning systems is not straightforward as we have chosen to use rigid phantoms in this initial work, whereas e.g. Gilles et al. [11] and Gaisberger et al. [10] analyzed the accuracy of their surface scanning system on patients, where the gold standard transformation was either a table shift or a manual registration of portal images to the planning CT. The performance of commercial systems AlignRT (VisionRT) and Catalyst (C-RAD) has been studied using anthropomorphic phantoms and is found to be < 1 mm/< 1° [28,4,29,30].

This work supplements similar studies by performing an offline fiducial marker registration procedure to compare the 6 DOF from the rigid registration to the ICP transformation. Gilles et al. [11] and Moser et al. [31] use 3 (or 4 resp.) DOF and are therefore limited in their accuracy evaluation. Furthermore, Gaisberger et al. [10] detected an improved registration accuracy for the translations when using the full 6 DOF compared to registration without rotation for breast cancer patients using an in-house developed surface scanning system.

We noted systematic errors for all three phantoms, distinct in the roll component for the hand and breast. As a validation, the performance of a commercial system was tested on these specific phantoms. We used AlignRT to position the phantoms on a TrueBeam (Varian, USA) in the same procedure as for the prototype validation. The phantoms were placed with a slight offset from the planned position and the AlignRT setup errors were compared to the kV-CBCT registration results. The AlignRT system had combined registration errors for our 3D-printed phantoms of lat: 0.7 ± 0.6 mm, vert: −0.6 ± 1.4 mm, long: 0.6 ± 0.8 mm and yaw: −0.3 ± 0.3°, pitch: −0.2 ± 0.3°, roll: 0.4 ± 0.3°. We suspect the non-zero results in both systems to be caused by the surface topography of the individual phantoms, as correct convergence of the ICP algorithm is highly dependent on features in the data [32].

Previous studies [11,33] on surface monitoring position the patient relative to a first reference surface, which is a 3D image acquired with the depth camera after initial positioning with X-ray image guidance. This approach could introduce a systematic error in subsequent fractions. On the other hand, both Moser et al. [31] and Pallotta et al. [34] noted an improved registration accuracy for the C-RAD Sentinel system when using an optical reference surface compared to the planning CT contours. We observed a decrease in systematic errors for the head phantom when using the captured reference surface, from 1.7 ± 0.4 mm to 0.4 ± 0.3 mm in the longitudinal translation. However, the largest RE was found for the captured reference for the breast phantom. The captured reference has the benefit of already providing information on a suitable region-of-interest, as parts not seen from the single camera viewpoint are already excluded. The capture however does not prevent the ICP registration from reaching a sub-optimal convergence due to specific surface topography. In our study it remains unclear which approach results in the highest accuracy.

The principal objective of the CISS was intra-bore motion monitoring, as initial patient positioning is less relevant in the confined space. The single depth camera prototype has been shown to have an adequate accuracy for small deviations from the planned position. However, as shown in Supplementary Fig. 3, the lateral sides of the phantoms could only partially be reconstructed from the single viewpoint. In the continuation of this work a second camera will be added – where both cameras are placed slightly off-axis – to increase the total

Table 2
Mean (± standard deviation) registration error of the surface scanning for the planning CT body contour and the surface capture reference (N = 24).

Phantom	Reference	Translation			Rotation		
		Lat (mm)	Vert (mm)	Long (mm)	Yaw (°)	Pitch (°)	Roll(°)
Head	Body contour	0.4 ± 0.7	0.3 ± 0.2	1.8 ± 0.4	−0.1 ± 0.5	0.7 ± 0.2	−0.3 ± 0.5
	Capture	−0.3 ± 0.7	−0.4 ± 0.2	0.4 ± 0.3	−0.3 ± 0.3	−0.2 ± 0.2	0.2 ± 0.5
Hand	Body contour	0.7 ± 0.6	−0.2 ± 0.3	0.4 ± 0.5	−0.7 ± 0.5	0.3 ± 0.3	1.0 ± 0.7
	Capture	0.2 ± 0.6	0.7 ± 0.3	−0.6 ± 0.6	−0.8 ± 0.5	0.7 ± 0.3	−1.0 ± 0.7
Breast	Body contour	1.1 ± 0.8	−0.4 ± 0.2	0.8 ± 0.5	−0.7 ± 0.6	1.2 ± 0.2	1.3 ± 0.8
	Capture	−1.9 ± 0.7	1.0 ± 0.2	0.6 ± 0.5	−1.5 ± 0.5	0.4 ± 0.3	−2.0 ± 0.7

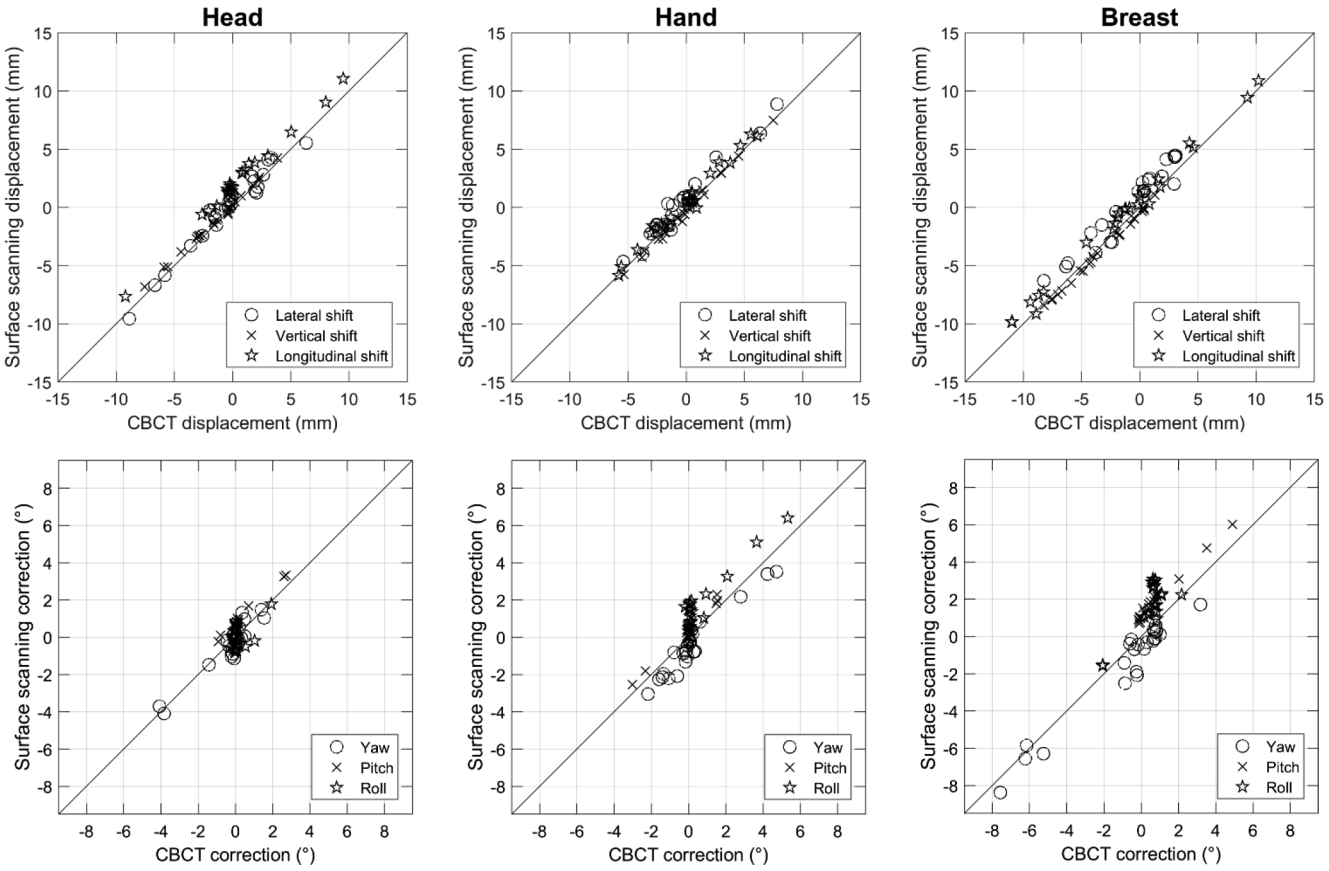

Fig. 3. Displacements detected by the surface scanning prototype compared to the MV-CBCT to CT registration value for the planning CT body contour reference surface. Diagonal line represents 1:1 relation. The top row displays the translations, bottom row the rotations.

body surface.

The current implementation of the software on a mid-tier computer resulted in a latency of around 1 s (ROI dependent), which is too high for breathing motion detection. Installing the software suite on more powerful computer hardware will decrease the latency.

In this paper a compact single-camera surface guidance system for intra-bore motion monitoring in O-ring gantries was developed and the accuracy investigated using anthropomorphic 3D-printed phantoms. This study shows the feasibility of intra-bore surface scanning in an O-ring bore providing comparable performance as ceiling mounted systems on C-arm linacs. This approach can be useful during extended fraction times in online adaptive workflows and SBRT or to monitor breath-hold stability.

Declaration of Competing Interest

This work is supported by Varian Medical Systems.

Appendix A. Supplementary data

Supplementary data to this article can be found online at https://doi.org/10.1016/j.phro.2019.07.003.

References

[1] Verellen D, Ridder M, Linthout N, Tournel K, Soete G, Storme G. Innovations in image-guided radiotherapy. Nat Rev Cancer 2007;12:949–60. https://doi.org/10.1038/nrc2288.
[2] Murphy MJ, Balter J, Balter S, Bencomo JA, Das IJ, Jiang SB, et al. The management of imaging dose during image-guided radiotherapy. Med Phys 2007;10:4041–63. https://doi.org/10.1118/1.2775667.
[3] Bert C, Metheany KG, Doppke KP, Taghian AG, Powell SN, Chen GTY. Clinical experience with a 3D surface patient setup system for alignment of partial-breast irradiation patients. Int J Radiat Oncol 2006;4:1265–74. https://doi.org/10.1016/j.ijrobp.2005.11.008.
[4] Peng JL, Kahler D, Li JG, Samant S, Yan G, Amdur R, et al. Characterization of a real-time surface image-guided stereotactic positioning system. Med Phys 2010;10:5421–33. https://doi.org/10.1016/j.ijrobp.2005.11.008.
[5] Wiant D, Liu H, Hayes TL, Shang Q, Mutic S, Sintay B. Direct comparison between

surface imaging and orthogonal radiographic imaging for SRS localization in phantom. J Appl Clin Med Phys 2019;1:137–44. https://doi.org/10.1002/acm2.12498.
[6] Stanley DN, McConnell KA, Kirby N, Gutiérrez AN, Papanikolaou N, Rasmussen K. Comparison of initial patient setup accuracy between surface imaging and three point localization. J Appl Clin Med Phys 2017;6:58–61. https://doi.org/10.1002/acm2.12183.
[7] Alderliesten T, Sonke JJ, Betgen A, Honnef J, van Vliet-Vroegindeweij C, Remeijer P. Accuracy evaluation of a 3-dimensional surface imaging system for guidance in deep-inspiration breath-hold radiation therapy. Int J Radiat Oncol 2013;2:536–42. https://doi.org/10.1016/j.ijrobp.2012.04.004.
[8] Betgen A, Alderliesten T, Sonke JJ, van Vliet-Vroegindeweij C, Bartelink H, Remeijer P. Assessment of set-up variability during deep inspiration breath hold radiotherapy for breast cancer patients by 3D-surface imaging. Radiother Oncol 2013;2:225–30. https://doi.org/10.1016/j.radonc.2012.12.016.
[9] Schönecker S, Walter F, Freislederer P, Marisch C, Scheithauer H, Harbeck N, et al. Treatment planning and evaluation of gated radiotherapy in left-sided breast cancer patients using the Catalyst(TM)/Sentinel(TM) system for deep inspiration breath-hold (DIBH). Radiat Oncol 2016;1:143. https://doi.org/10.1186/s13014-016-0716-5.
[10] Gaisberger C, Steininger P, Mitterlechner B, Huber S, Weichenberger H, Sedlmayer F, et al. Three-dimensional surface scanning for accurate patient positioning and monitoring during breast cancer radiotherapy. Strahlenther Onkol 2013;10:887–93. https://doi.org/10.1007/s00066-013-0358-6.
[11] Gilles M, Fayad H, Miglierini P, Clement JF, Scheib S, Cozzi L, et al. Patient positioning in radiotherapy based on surface imaging using time of flight cameras. Med Phys 2016;8:4833. https://doi.org/10.1118/1.4959536.
[12] Heß M, Büther F, Gigengack F, Dawood M, Schäfers KP. A dual-Kinect approach to determine torso surface motion for respiratory motion correction in PET. Med Phys 2015;5:2276–86. https://doi.org/10.1118/1.4917163.
[13] Noonan PJ, Howard J, Hallett WA, Gunn RN. Repurposing the Microsoft Kinect for Windows v2 for external head motion tracking for brain PET. Phys Med Biol 2015;22:8753–66. https://doi.org/10.1088/0031-9155/60/22/8753.
[14] Edmunds DM, Gothard L, Khabra K, Kirby A, Madhale P, McNair H, et al. Low-cost Kinect Version 2 imaging system for breath hold monitoring and gating. J Appl Clin Med Phys 2018;3:71–8. https://doi.org/10.1002/acm2.12286.
[15] Xia J, Siochi RA. A real-time respiratory motion monitoring system using KINECT. Med Phys 2012;5:2682–5. https://doi.org/10.1118/1.4704644.
[16] Padilla L, Pearson EA, Pelizzari CA. Collision prediction software for radiotherapy treatments. Med Phys 2015;11:6448–56. https://doi.org/10.1118/1.4932628.
[17] Torr PHS, Zisserman A. MLESAC. Comput Vis Image Und 2000;1:138–56. https://doi.org/10.1006/cviu.1999.0832.
[18] Besl PJ, McKay ND. A method for registration of 3-D shapes. IEEE T Pattern Anal 1992;2:239–56. https://doi.org/10.1109/34.121791.
[19] Birdal T. ICP Registration using Efficient Variants and Multi-Resolution Scheme. https://nl.mathworks.com/matlabcentral/fileexchange/47152-icp-registration-using-efficient-variants-and-multi-resolution-scheme. Accessed March 12, 2015.
[20] Zinsser T, Schmidt J, Niemann H. A refined ICP algorithm for robust 3-D correspondence estimation. Proc 2003 Int Conf Im Process 2003:II-695-8. https://doi.org/10.1109/ICIP.2003.1246775.
[21] Adult Human Head. Available at: https://grabcad.com/library/adult-human-head-1. Accessed May 8, 2018.
[22] Arm by Artec3D. Available at: https://www.artec3d.com/3d-models/arm. Accessed May 23, 2018.
[23] Duda RO, Hart PE. Use of the Hough transformation to detect lines and curves in pictures. Commun ACM 1972;1:11–5. https://doi.org/10.1145/361237.361242.
[24] Xie L. Spherical hough transform for 3D images. Available at: https://nl.mathworks.com/matlabcentral/fileexchange/48219-spherical-hough-transform-for-3d-images. Accessed May 10, 2018.
[25] Horn BKP. Closed-form solution of absolute orientation using unit quaternions. J Opt Soc Am 1987;4:629. https://doi.org/10.1364/JOSAA.4.000629.
[26] Fedorov A, Beichel R, Kalpathy-Cramer J, Finet J, Fillion-Robin JC, Pujol S, et al. 3D Slicer as an image computing platform for the Quantitative Imaging Network. Magn Reson Imaging 2012;9:1323–41. https://doi.org/10.1016/j.mri.2012.05.001.
[27] Willoughby T, Lehmann J, Bencomo JA, Jani SK, Santanam L, Sethi A, et al. Quality assurance for nonradiographic radiotherapy localization and positioning systems. Med Phys 2012;4:1728–47. https://doi.org/10.1118/1.3681967.
[28] Bert C, Metheany KG, Doppke K, Chen GTY. A phantom evaluation of a stereo-vision surface imaging system for radiotherapy patient setup. Med Phys 2005;9:2753–62. https://doi.org/10.1118/1.1984263.
[29] Wiencierz M, Kruppa K, Lüdemann L. Clinical validation of two surface imaging systems for patient positioning in percutaneous radiotherapy. http://arxiv.org/pdf/1602.03749v1.
[30] Belge D, Godron F. Quality assurance program for Catalyst™, a 3D surface imaging system for patient setup verification in radiotherapy. Phys Medica 2013:e4–5. https://doi.org/10.1016/j.ejmp.2013.08.015.
[31] Moser T, Habl G, Uhl M, Schubert K, Sroka-Perez G, Debus J, et al. Clinical evaluation of a laser surface scanning system in 120 patients for improving daily setup accuracy in fractionated radiation therapy. Int J Radiat Oncol 2013;3:846–53. https://doi.org/10.1016/j.ijrobp.2012.05.026.
[32] Rusinkiewicz S, Levoy M. Efficient variants of the ICP algorithm. Proc Third Int Conf 3D Dig Imaging Modelling Québec 2001:145–52. https://doi.org/10.1109/IM.2001.924423.
[33] Placht S, Stancanello J, Schaller C, Balda M, Angelopoulou E. Fast time-of-flight camera based surface registration for radiotherapy patient positioning. Med Phys 2012;1:4–17. https://doi.org/10.1118/1.3664006.
[34] Pallotta S, Marrazzo L, Ceroti M, Silli P, Bucciolini M. A phantom evaluation of Sentinel(™), a commercial laser/camera surface imaging system for patient setup verification in radiotherapy. Med Phys 2012;2:706–12. https://doi.org/10.1118/1.3675973.